

SANDIA REPORT

SAND2017-10085

Unlimited Release

Printed September 2017

ATLOG Modeling of Aerial Cable from the November 2016 HERMES Electromagnetic Pulse Experiments

Salvatore Campione, Larry K. Warne, Benjamin T. Yee, Keith L. Cartwright, and Lorena I. Basilio

Prepared by
Sandia National Laboratories
Albuquerque, New Mexico 87185 and Livermore, California 94550

Sandia National Laboratories is a multimission laboratory managed and operated by National Technology and Engineering Solutions of Sandia, LLC., a wholly owned subsidiary of Honeywell International, Inc., for the U.S. Department of Energy's National Nuclear Security Administration under contract DE-NA-0003525.

Approved for public release; further dissemination unlimited.



Sandia National Laboratories

Issued by Sandia National Laboratories, operated for the United States Department of Energy by Sandia Corporation.

NOTICE: This report was prepared as an account of work sponsored by an agency of the United States Government. Neither the United States Government, nor any agency thereof, nor any of their employees, nor any of their contractors, subcontractors, or their employees, make any warranty, express or implied, or assume any legal liability or responsibility for the accuracy, completeness, or usefulness of any information, apparatus, product, or process disclosed, or represent that its use would not infringe privately owned rights. Reference herein to any specific commercial product, process, or service by trade name, trademark, manufacturer, or otherwise, does not necessarily constitute or imply its endorsement, recommendation, or favoring by the United States Government, any agency thereof, or any of their contractors or subcontractors. The views and opinions expressed herein do not necessarily state or reflect those of the United States Government, any agency thereof, or any of their contractors.

Printed in the United States of America. This report has been reproduced directly from the best available copy.

Available to DOE and DOE contractors from

U.S. Department of Energy
Office of Scientific and Technical Information
P.O. Box 62
Oak Ridge, TN 37831

Telephone: (865) 576-8401
Facsimile: (865) 576-5728
E-Mail: reports@osti.gov
Online ordering: <http://www.osti.gov/scitech>

Available to the public from

U.S. Department of Commerce
National Technical Information Service
5301 Shawnee Rd
Alexandria, VA 22312

Telephone: (800) 553-6847
Facsimile: (703) 605-6900
E-Mail: orders@ntis.gov
Online order: <http://www.ntis.gov/search>



SAND2017-10085
Unlimited Release
Printed September 2017

ATLOG Modeling of Aerial Cable from the November 2016 HERMES Electromagnetic Pulse Experiments

Salvatore Campione, Larry K. Warne, Keith L. Cartwright, and Lorena I. Basilio
Electromagnetic Theory

Benjamin T. Yee
Applied Optical/Plasma Science

Sandia National Laboratories
P.O. Box 5800
Albuquerque, New Mexico 87185-1152

Abstract

This report details the comparison of ATLOG modeling results for the response of a finite-length dissipative aerial conductor interacting with a conducting ground to a measurement taken November 2016 at the High-Energy Radiation Megavolt Electron Source (HERMES) facility. We use the ATLOG time-domain method based on transmission line theory. Good agreement is observed between simulations and experiments.

Intentionally Left Blank

CONTENTS

1. Introduction.....	7
2. DATA AVAILABLE FROM THE NOVEMBER 2016 HERMES EXPERIMENT FROM SHOT 10298	9
3. MODELING OF THE AERIAL CABLE IN THE NOVEMBER 2016 HERMES EXPERIMENT FROM SHOT 10298	11
4. CONCLUSIONS	17
REFERENCES	17
Distribution	18

FIGURES

Figure 1. Schematic of shot 10298 of the November 2016 HERMES experiment. The wires are along the z -direction and only a cross section is shown for simplicity.	9
Figure 2. Electric field at three different locations along the cable as dictated by Eq. (2).	11
Figure 3. Comparison of the electric field obtained from the model in Eq. (2) for the field at the 3DZ probe location scaled to the 4DZ location with what actually measured at the 4DZ probe location.	12
Figure 4. Current versus time for a 12 m long ibis cable with lossy ground and no air conductivity. Results are based on the time-domain ATLOG model and the experimental data. The current is evaluated at $z = 7.47$ m.	13
Figure 5. Current versus time for a 12 m long ibis cable with lossy ground, $\sigma_g = 0.01$ S/m, and two-region air conductivity as in Eq. (3). Results are based on the time-domain ATLOG model and the experimental data. The current is evaluated at $z = 7.47$ m.	14
Figure 6. Current versus time for a 12 m long ibis cable with lossy ground, $\sigma_g = 0.0015$ S/m, and two-region air conductivity as in Eq. (3). Results are based on the time-domain ATLOG model and the experimental data. The current is evaluated at $z = 7.47$ m.	14
Figure 7. Current versus time as in Figure 6, for three conditions of the wire conductivity, specifically PEC, DC, and high-frequency. Results are based on the time-domain ATLOG model. The current is evaluated at $z = 7.47$ m.	15

Intentionally Left Blank

1. INTRODUCTION

The purpose of this report is to provide a comparison of results for the current induced on finite-length dissipative aerial conductors interacting with a conducting ground when excited by an electromagnetic pulse (EMP). We consider the following two environments:

1. November 2016 experiments taken at the High-Energy Radiation Megavolt Electron Source (HERMES) facility [1];
2. Time-domain ATLOG model based on transmission line theory, whose formulation can be found in [2-3].

The goal is to identify the minimal set of information required to simulate the current on the aerial cable. This is important due to great uncertainty in some of the parameters during the experiment.

2. DATA AVAILABLE FROM THE NOVEMBER 2016 HERMES EXPERIMENT FROM SHOT 10298

We concentrate on shot 10298 of the November 2016 HERMES EMP experiment [4]. The configuration layout is schematically reported in Figure 1. Both buried and aerial cables are present, but only aerial cables will be investigated in this report; buried cables will be analyzed in a future effort.

The cables of interest are ibis-class aluminum conductor steel-reinforced (ACSR) cables, 12 m long and left open-circuited at both terminations. In the aerial case, the cable is at a height of 0.88 m. There are three electric field probes (3DZ, 4DZ, and 6DZ) that collect the EMP exciting field and time dependence. There are also current measurement probes located at the center of the buried cable and at $z = 7.47$ m for the aerial cable.

Since the excitation field is measured with all the cables present in Figure 1, we decided to consider only the aerial ibis cable and ignore the effects from other cables nearby. Also, note the ibis cable is closest to the ground, which introduces some isolation from the other cables. Finally, the ibis cable is double the length of the other cables.

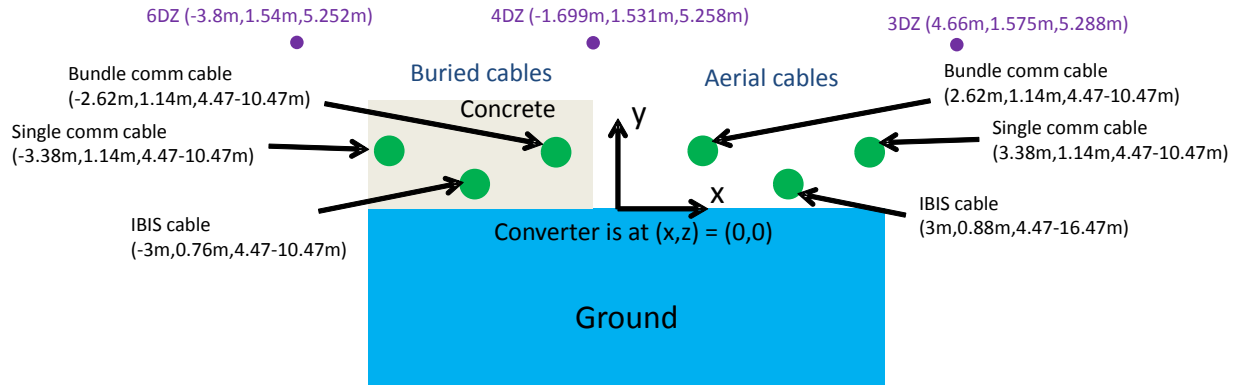


Figure 1. Schematic of shot 10298 of the November 2016 HERMES experiment. The wires are along the z-direction and only a cross section is shown for simplicity.

3. MODELING OF THE AERIAL CABLE IN THE NOVEMBER 2016 HERMES EXPERIMENT FROM SHOT 10298

In this section we report the modeling of the aerial cable in the environment reported in Figure 1. First of all, we use the measured electric fields (3DZ, 4DZ, and 6DZ) from the trials as the source term for the ATLOG model. The 12m-long ibis cable is assumed to have $\varepsilon_2 = \varepsilon_0$ (i.e. no coating), radius $a = b = 0.3915$ inches, and a DC solid wire conductivity $\sigma_0 = 2.3 \times 10^7$ S/m. The

DC resistance is fixed at $R = \frac{1}{\pi a^2 \sigma_0}$. Note that this value does not really represent the true

dynamic internal impedance per unit length of the wire. We will assess its effect in the final figure of the report. The cable is left open-circuited at both ends. We use the data from the 3DZ probe as the source term for the ibis cable. As the probe is located above the wire, we impose a linear approximation of the field approaching the ground. Therefore, along the wire, the field should be scaled as

$$E_z(r_y, t) = \frac{y}{y_0} E_z(r_0, t) \quad (1)$$

where y is the height of the cable at position r_y , and y_0 is the y -location of the 3DZ probe at position r_0 , and $E_z(r_0, t)$ is the time dependence of the field at the measurement point r_0 .

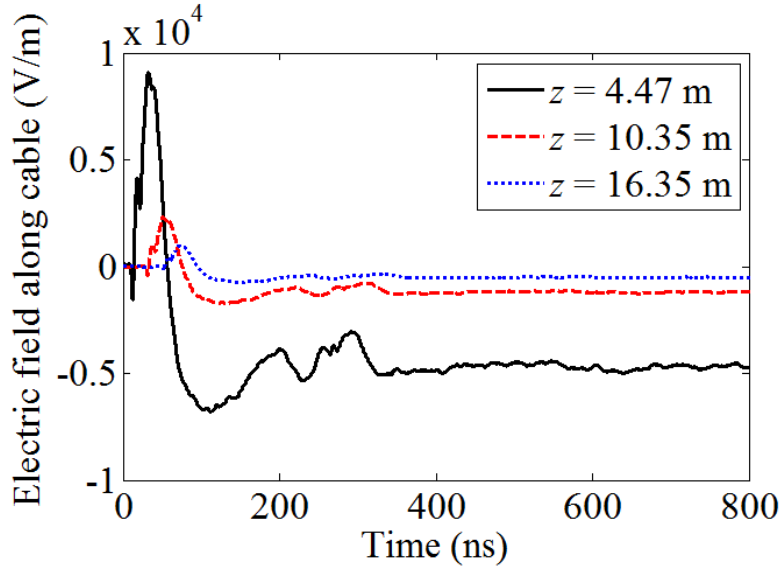


Figure 2. Electric field at three different locations along the cable as dictated by Eq. (2).

While this correction takes the field to the cable height, it still needs to be distributed along the cable length, which runs from 4.47 m to 16.47 m (this requires both a scaling and a delay along the line). We take this distribution as

$$E_z(r, t) = \frac{r_0^2}{r^2} E_z\left(r_y, t - \frac{r}{c}\right), \quad (2)$$

where r is the locus of points along the cable and c the speed of light. The excitation field at three different locations along the cable as dictated by Eq. (2) is reported in Figure 2. One can see that for increasing distance from the source (located at the origin of the reference system) the field is both attenuated and delayed.

To show that the model in Eq. (2) is reasonable, we apply it to predict the fields measured by 4DZ using the 3DZ data, and compare it to the actual 4DZ measurements. This result is shown in Figure 3. The agreement between the two curves shown in Figure 3 indicates that Eq. (2) can be used to model the field along the ibis cable. The scaling difference of about 1.35 between the two curves could be due to measurement artifacts.

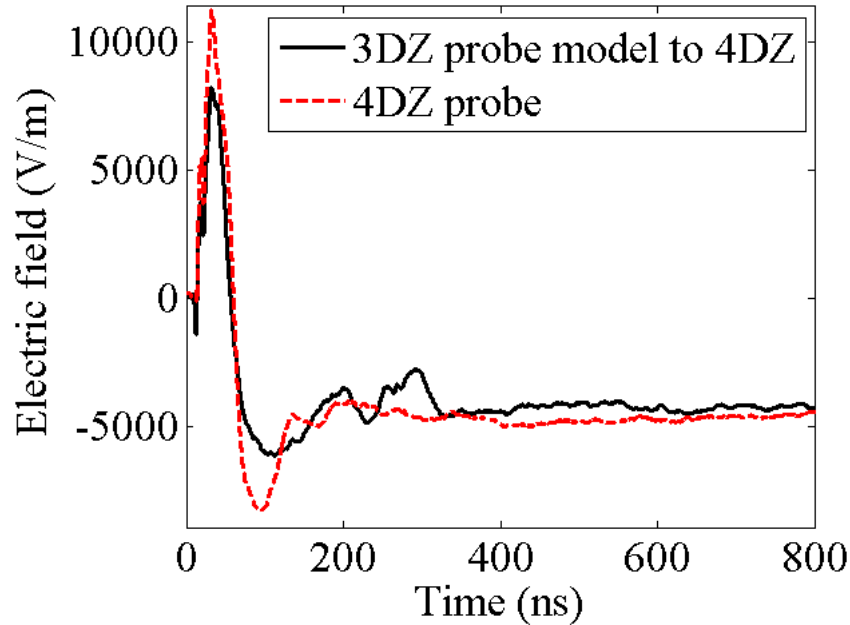


Figure 3. Comparison of the electric field obtained from the model in Eq. (2) for the field at the 3DZ probe location scaled to the 4DZ location with what actually measured at the 4DZ probe location.

Guided by the experimental data [4], the parameters we first take in this section on the simulations are as follows: lossy ground with $\epsilon_g = 3\epsilon_0$ (i.e. concrete) and $\sigma_g = \{0.0015, 0.01\}$ S/m, no air conductivity. We report the current at $z = 7.47$ m for the two ground conductivity cases in Figure 4, and compare the two results with the experimental data. One can see that the result for $\sigma_g = 0.01$ S/m shows an oscillatory behavior with similar frequency content as observed in the experiment, but with slower decay rate. The decay rate is improved by considering $\sigma_g = 0.0015$ S/m. However, a careful look at the data shows that the highest current peak is not accurately predicted, which suggests the presence of air conductivity

in the early radiation phase of the pulse. We also want to mention that considering $\varepsilon_g = 10\varepsilon_0$ instead of $\varepsilon_g = 3\varepsilon_0$ would produce a small effect on the current results (not shown).

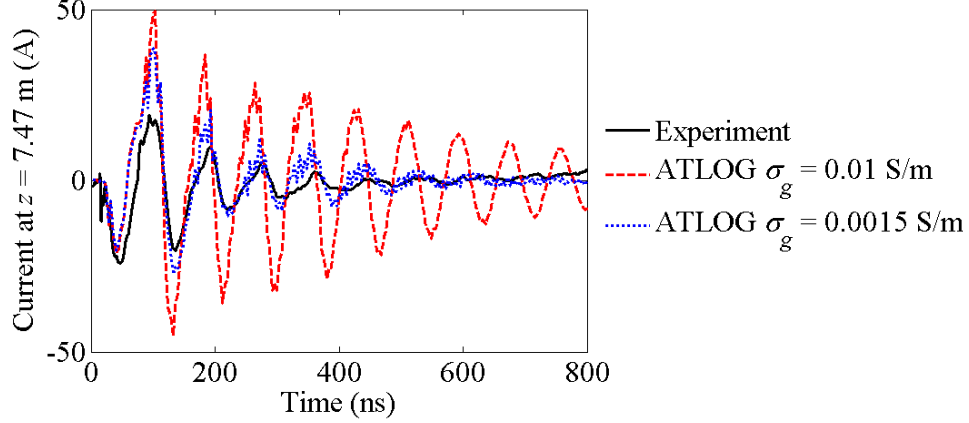


Figure 4. Current versus time for a 12 m long ibis cable with lossy ground and no air conductivity. Results are based on the time-domain ATLOG model and the experimental data. The current is evaluated at $z = 7.47$ m.

Indeed, a careful look at the experimental data [5] shows the presence of air conductivity at early times. Following what reported in [5], we study two scenarios:

$$\begin{aligned} \text{Case 1: } \sigma_{\text{air}} &= \begin{cases} 4 \times 10^{-4} \text{ S/m} & t < 80 \text{ ns} \\ 1 \times 10^{-6} \text{ S/m} & t \geq 80 \text{ ns} \end{cases} \\ \text{Case 2: } \sigma_{\text{air}} &= \begin{cases} 4 \times 10^{-4} \text{ S/m} & t < 80 \text{ ns} \\ 0 \text{ S/m} & t \geq 80 \text{ ns} \end{cases} \end{aligned} \quad (3)$$

It will be shown that the air conductivity value at later times (i.e. $t \geq 80$ ns) will not affect the reported predictions. Indeed, the use of $\sigma_{\text{air}} = 5 \times 10^{-6}$ S/m for $t \geq 80$ ns does not show significant effects (not shown).

We report in Figure 5 the current for the case of $\sigma_g = 0.01$ S/m, accounting for the two-region air conductivity model discussed in Eq. (3). One can see that, even with the presence of both ground losses and air losses, the decay rate is too slow to match with the experimental data. However, the inclusion of a non-zero air conductivity has reduced the peak current from 50 A to approximately 30 A, better matching the measurements.

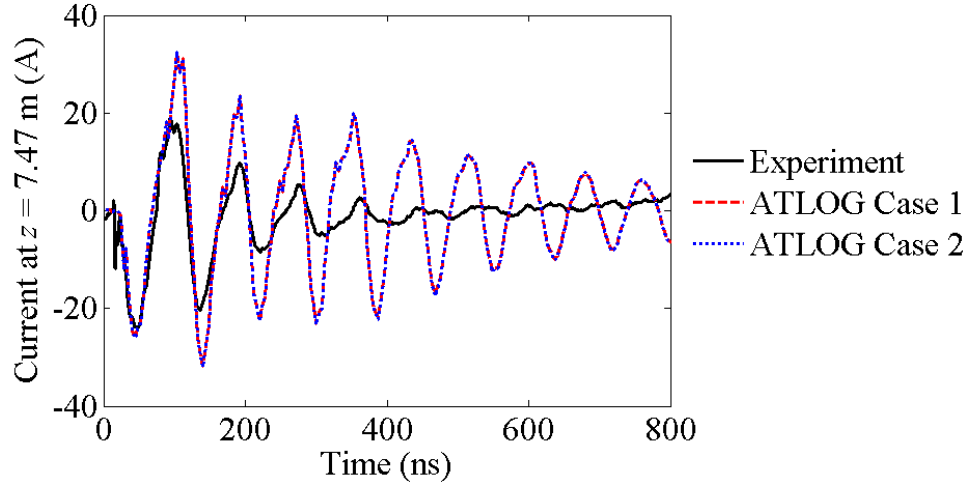


Figure 5. Current versus time for a 12 m long ibis cable with lossy ground, $\sigma_g = 0.01$ S/m, and two-region air conductivity as in Eq. (3). Results are based on the time-domain ATLOG model and the experimental data. The current is evaluated at $z = 7.47$ m.

We report in Figure 6 the current for the case of $\sigma_g = 0.0015$ S/m accounting for the two-region air conductivity model discussed in Eq. (3). In this case, the decay rate well matches the experimental data and the highest peak is well predicted by the simulation.

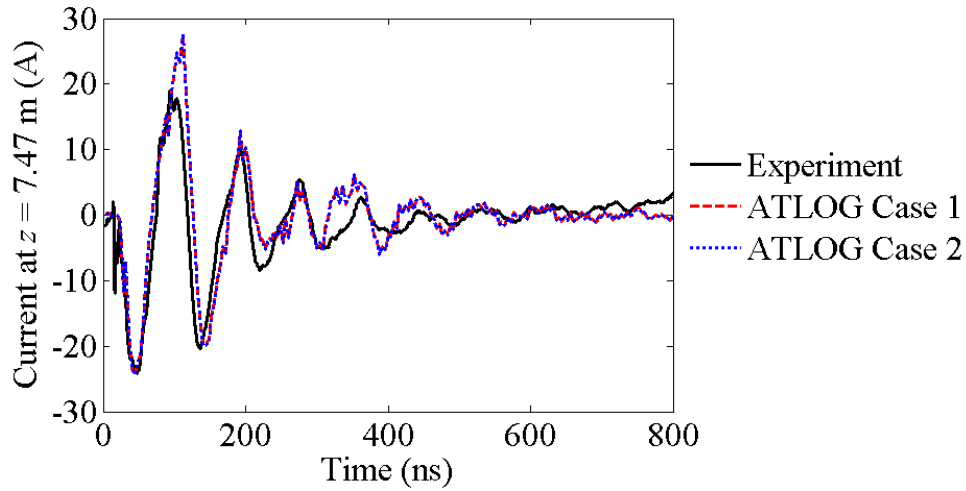


Figure 6. Current versus time for a 12 m long ibis cable with lossy ground, $\sigma_g = 0.0015$ S/m, and two-region air conductivity as in Eq. (3). Results are based on the time-domain ATLOG model and the experimental data. The current is evaluated at $z = 7.47$ m.

All the previous analyses were based on a DC conductivity for the solid wire. We now consider also the high frequency resistance of a solid wire $\frac{R_s}{2\pi a} = \frac{1}{\pi a^2 \sigma_{\text{eff}}}$, with $R_s = \frac{1}{\sigma_0 \delta}$ and $\delta = \sqrt{\frac{2}{\omega \mu_0 \sigma_0}}$. This leads to an effective conductivity $\sigma_{\text{eff}} = 2.1 \times 10^5 \text{ S/m}$. We also consider the case of a perfect electric conductor (PEC) wire. The current for these three cases is shown Figure 7. Even though there are complications due to stranding and inner steel core, the comparison of these three cases shows that, over this time scale, the dominant losses are the ground, and the cable losses are negligible.

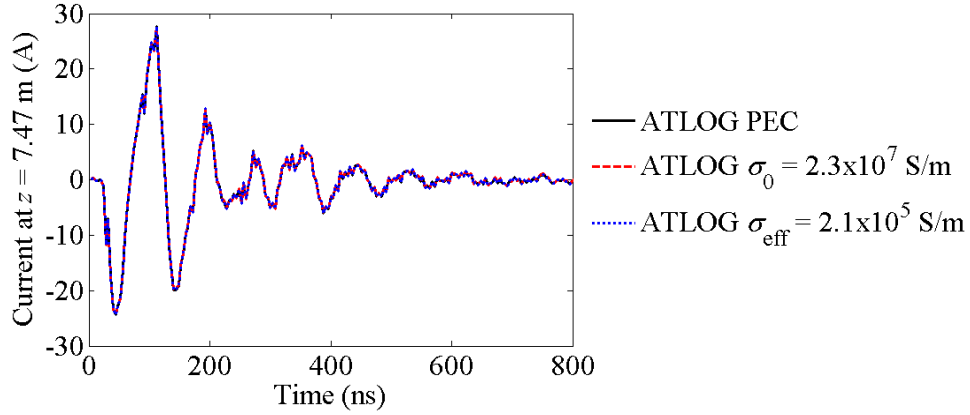


Figure 7. Current versus time as in Figure 6, for three conditions of the wire conductivity, specifically PEC, DC, and high-frequency. Results are based on the time-domain ATLOG model. The current is evaluated at $z = 7.47 \text{ m}$.

4. CONCLUSIONS

In this report we presented model results for the current induced on finite-length aerial conductors interacting with a conducting ground as in the November 2016 HERMES environment. We used the time-domain ATLOG model to compare to the experiment. Good agreement has been observed for aerial cables. Compared to the damping from the ground, it appears like the air conductivity is important for the early radiation phase of the pulse, and plays small role at later times. As an outcome of the ATLOG model, we have identified the minimal set of information required to simulate the current on the aerial cable. This is important due to great uncertainty in some of the less important parameters (e.g. late-time air conductivity) during the experiment.

REFERENCES

- [1] G. A. Zawadzkas, “The HERMES-III Gamma-Ray Facility at the Simulation Technology Laboratory-A Guide for Users,” *Sandia National Laboratories Report*, vol. SAND89-0481, Albuquerque, New Mexico 87185 and Livermore, California 94550, 1989.
- [2] S. Campione, L. K. Warne, R.L. Schiek, and L. I. Basilio, “Electromagnetic Pulse Excitation of Finite-Long Dissipative Conductors over a Conducting Ground Plane in the Time Domain,” *Sandia National Laboratories Report*, vol. SAND2017-10085, Albuquerque, NM, 2017.
- [3] S. Campione, L. K. Warne, R.L. Schiek, and L. I. Basilio, “Comparison of ATLOG and Xyce for Bell Labs Electromagnetic Pulse Excitation of Finite-Long Dissipative Conductors over a Ground Plane,” *Sandia National Laboratories Report*, vol. SAND2017-10085, Albuquerque, NM, 2017.
- [4] B. T. Yee, K. L. Cartwright, and T. D. Pointon, “November 2016 WESC Trials: Free Space Fields and Current Coupling,” *Sandia National Laboratories Report*, vol. SAND2017-10085, Albuquerque, NM, 2017.
- [5] B. T. Yee and K. L. Cartwright, “November 2016 WESC Trials: Air Conductivity Measurements,” *Sandia National Laboratories Report*, vol. SAND2017-10085, Albuquerque, NM, 2017.

DISTRIBUTION

Number	Mail Stop	Name	Dept.
1 (electronic)	MS0492	K. C. Chen	9411
1 (electronic)	MS0899	Technical Library	9536
1 (electronic)	MS1152	G. Pena	1350
3	MS1152	S. Campione	1352
3	MS1152	L. K. Warne	1352
3	MS1152	L. I. Basilio	1352
1 (electronic)	MS1152	S. Campione	1352
1 (electronic)	MS1152	L. K. Warne	1352
1 (electronic)	MS1152	L. I. Basilio	1352
1 (electronic)	MS1152	K. L. Cartwright	1352
1 (electronic)	MS1152	K. Sainath	1352
1 (electronic)	MS1168	L. X. Schneider	1350
1 (electronic)	MS1173	L. D. Bacon	5443
1 (electronic)	MS1173	M. J. Walker	5443
1 (electronic)	MS1177	R. L. Schiek	1355
1 (electronic)	MS1177	J. P. Castro	1355
1 (electronic)	MS1189	R. B. Campbell	1641
1 (electronic)	MS1423	B. T. Yee	1868
1 (electronic)	MS9007	C. Lam	8115

